Atomic Force Microscopy and Infrared Spectroscopy Studies of the Thermal Degradation of Nomex Aramid Fibers

S. Villar-Rodil, J. I. Paredes, A. Martínez-Alonso,* and J. M. D. Tascón

Instituto Nacional del Carbón, CSIC, Apartado 73, 33080 Oviedo, Spain

Received November 9, 2000. Revised Manuscript Received May 7, 2001

In the present work, the thermal transformations of Nomex [poly(*m*-phenylene isophthalamide)] fibers have been investigated up to a temperature of 1173 K. The main stages of the pyrolytic degradation of the fibers were determined by thermal analysis, and their chemical and morphological evolution through the different steps was subsequently followed by Fourier transform infrared spectroscopy (FTIR) and atomic force microscopy (AFM) measurements, respectively. The degradation starts with the cleaving of hydrogen bonds at approximately 633 K, which leads to a disordering of the polyaramide chains on the nanometer scale. The next decomposition step takes place between 673 and 873 K with the disruption of the amide bonds, the subsequent breaking of the polyaramide chains into smaller units, and their condensation into large polyaromatic compounds. From 873 K onward, the reaction progresses by the dehydrogenation of the polyaromatic structures and their arrangement into graphite-like assemblies, resulting in the final fibrous carbon which is obtained at 1173 K.

1. Introduction

Aramid fibers are a class of synthetic polymers which possess excellent thermal and oxidative stability, flame resistance, and superior mechanical and dielectric behavior.[1] It is for these reasons that they have found increasing uses in a wide variety of demanding applications in modern technology. One of these applications takes advantage of their thermal stability and allows the manufacturing of heat-resistant materials for fire protection.[2] In a different context, aramid fibers have been proposed in the last years as precursors of activated carbon materials with distinctive adsorbent properties, such as molecular sieve behavior.[3−5] The high crystallinity of this type of fiber is an important advantage for this purpose, which sets them apart from the usual fibrous precursors of low or intermediate crystallinity. In this case, the aramid fibers are normally transformed into activated carbon fibers by a two-step process: pyrolysis and (physical) activation. In consequence, the study of the thermal transformation of aramid fibers has relevance in, on one hand, understanding the mechanisms by which the fiber degrades and, on the other hand, being able to select the most advantageous conditions to prepare activated carbon fibers.

The thermal degradation of aramid fibers has been investigated in the past through the analysis of the compounds evolved during their pyrolysis by techniques such as infrared spectroscopy, gas chromatography, or mass spectrometry.[6−11] These studies provided valuable indirect information on the chemistry of the degradation process of aramids. However, direct information on the changes undergone by the solid material upon pyrolysis is still lacking or is very rare. As a matter of fact, very few examples are reported in the literature[8,11−14] and most of them concern Kevlar, poly(*p*-phenylene terephthalamide).

The main objective of this work was to get an insight into the chemical and morphological transformations undergone by the poly(*m*-phenylene isophthalamide) fiber known as Nomex upon pyrolysis up to 1173 K, when the polymer has been completely transformed into

* To whom correspondence should be addressed. Tel: (+34) 985 11 90 90. Fax: (+34) 985 29 76 62. E-mail: amelia@incar.csic.es.

(1) Yang, H. H. *Aromatic High Strength Fibers*; John Wiley & Sons: New York, 1989.
(2) Pilato, L. A.; Michno, M. J. *Advanced Composite Materials*; Springer-Verlag: Berlin, 1994.
(3) Freeman, J. J.; Gimblett, F. G. R.; Hayes, R. A.; Amin, Z. M.; Sing, K. S. W. In *Characterization of Porous Solids II*; Rodriguez-Reinoso F., Rouquerol J., Sing K. S. W., Eds.; Elsevier: Amsterdam, 1991; p 319.
(4) Freeman, J. J.; Tomlison, J. B.; Sing, K. S. W.; Theocaris, C. R. *Carbon* **1993**, *31*, 865.
(5) Freeman, J. J.; Tomlison, J. B.; Sing, K. S. W.; Theocaris, C. R. *Carbon* **1995**, *33*, 795.
(6) Krasnov, Y. P.; Savikov, V. M.; Sokolov, L. B.; Logunova, V. I.; Belyarov, V. K.; Polyakova, T. A. *Polym. Sci. U.S.S.R.* **1966**, *8*, 413.
(7) Kalashnik, A. T.; Panikarova, N. P.; Dovbii, Y. V.; Kozhina, G. V.; Kalmykova, V. D.; Papkov, S. P. *Vysokomol. Soedin.* **1977**, *12*, 2747.
(8) Khanna, Y. P.; Pearce, E. M.; Smith, J. S.; Burkitt, D. T.; Njuguna, H.; Hinderlang, D. M.; Forman, B. D. *J. Polym. Sci., Polym. Chem.* **1981**, *19*, 2817.
(9) Brown, J. R.; Power, A. J. *Polym. Degrad. Stab.* **1982**, *4*, 379.
(10) Schulten, H. R.; Plage, B.; Ohtani, H.; Tsuge, S. *Makromol. Chem.* **1987,** *155*, 1.
(11) Carroccio, S.; Puglisi, C.; Montaudo, G. *Macromol. Chem. Phys.* **1999**, *200*, 2345.
(12) Tomikuza, I.; Isoda, Y.; Amamiya, A. *Tanso* **1981**, *106*, 93.
(13) Mosquera, M. E. G.; Jamond, M.; Martínez-Alonso, A.; Tascon, J. M. D. *Chem. Mater.* **1994**, *6*, 1918.
(14) Yoon, S. H.; Kim, B. C.; Korai, I; Mochida, I. Biennial Conference on Carbon. Extended Abstracts and Program, 22nd, San Diego, CA, 1995; pp 218−219.

10.1021/cm001219f CCC: $20.00
Published on Web 10/24/2001

fibrous carbon. To date, the only direct available information about the thermal transformation of this polymer is essentially the elemental composition of the solid residue.[11,14] In the present work, Fourier transform infrared spectroscopy (FTIR) and atomic force microscopy (AFM) measurements have been carried out at different stages of the pyrolytic transformation of the fiber, selected by thermal analysis (TGA/DTG/DTA), to provide direct information about the changes taking place in the chemical bondings of the polymer (FTIR) and how those chemical changes affected the fiber surface morphology at the nanometer scale (AFM). The utility of FTIR to follow the thermal transformations of other polymeric materials during pyrolysis has been demonstrated in the past in a number of examples.[15−18] On the contrary, the application of AFM to monitor the morphological changes induced by pyrolysis on a polymer at different steps of the process is much less common, though some related work can be found in the literature.[19−22] Being an extremely surface-sensitive technique (capable of atomic or molecular resolution in the most favorable cases) and having proved its capabilities for the study of a wide range of materials,[23−27] AFM appears as a promising technique for this purpose. As will be shown thereafter, the morphological changes in the fibers during the different steps of pyrolysis are in general too subtle to be detected by more conventional microscopic techniques, such as scanning electron microscopy (SEM).

2. Experimental Section

The starting material employed was commercial poly(*m*-phenylene isophthalamide) fiber, known as Nomex, manufactured by DuPont. For the present study, a variety named Crystalline Nomex (Dtf 2.2) was used.

A Stanton-Redcroft STA-1500 thermobalance provided with a Plus-V software was used for simultaneous thermogravimetry (TG) /differential thermal analysis (DTA) measurements. The derivative of the TG curve (DTG) is also presented. The fibers were used as received in all the thermal treatments, without drying. Samples (∼10 mg) were placed in Pt crucibles that were 5 mm in diameter and 5 mm in height. A constant flow of 50 cm^3 min^{-1} of argon (99.99990% pure by volume) was used. Temperatures were measured with Pt/Rh thermocouples placed at the bottom of the Pt crucibles, in contact with them. α-Alumina was the reference material for DTA measurements. Several linear heating rates ranging from 5 to 40 K min^{-1} were tested over the temperature interval of 298−1173 K. Once a convenient heating rate was chosen, samples that were pyrolyzed to different selected temperatures were prepared in the same thermobalance under the same conditions, effectively stopping the process by rapid cooling to room temperature. These samples were considered to be representative of the different decomposition stages that the material undergoes.

Elemental analyses of all samples were carried out in a LECO CHNS-932 microanalysis apparatus with a LECO VTF-900 accessory for oxygen. FTIR absorption spectra were obtained in a Nicolet Magna IR560 spectrometer. Pellets in KBr with a sample concentration of $(2-5) \times 10^{-1}$ wt %, weighing 120 mg and 13 mm in diameter, were used. The spectra shown are the result of coadding 200 interferograms obtained at a resolution of 4 cm^{-1} and normalized to 1 mg cm^{-2}. All samples, fresh and pyrolyzed, were cold-ground at 77 K in a mixer mill used in combination with a cooling attachment in which liquid nitrogen was the coolant. Then, they were kept in a desiccator, avoiding direct exposure to sunlight in order to prevent their photochemical degradation.[28]

AFM investigations of the different heat-treated samples were carried out in air at room temperature with a Nanoscope Multimode IIIa from Digital Instruments. In every case, bundles of the fibers were attached to the AFM sample holder by means of adhesive tape, taking special care to avoid the presence of fibers protruding a great length from the sample surface which could interfere with the cantilever and prevent the attainment of stable imaging. The tapping mode of operation[29,30] was chosen over the more conventional contact mode to follow the morphological evolution of the fiber with heat treatment temperature. This was due to the fact that the cantilevers employed in tapping mode (made of etched Si, resonant frequency ≈ 250 kHz) have a considerably smaller tip radius of curvature (5−10 nm) than those used for contact mode and also that the lateral shear forces in the former mode are greatly reduced as compared with those of the latter, resulting in a better resolution of nanometer-sized features.[31] Particular attention was paid to minimize the tip−sample interaction during the tapping mode AFM measurements, this being necessary to obtain accurate surface topographic information.[32] To confirm the reproducibility of the images, several different previously unused tips were employed to study the samples, every sample was imaged on many different fibers, and every fiber was imaged on several different areas. All the images shown here were flattened and then smoothed by a low-pass filter to improve their visual presentation, taking special care to ensure that no artifacts or distortions were introduced by this procedure.

3. Results

3.1. Determination of the Main Stages of Pyrolysis: Thermal Analysis Studies. Figures 1 and 2 show some of the TG and DTA curves, respectively, obtained by varying the heating rate in the pyrolysis process. Apparently, changing this parameter does not modify the mechanism of pyrolysis: the TG curves keep their shape and simply shift to higher temperatures with increasing heating rates, resulting in higher yields, and all the DTA curves show the same features. Therefore, an intermediate heating rate of 10 K min^{-1} was chosen (part b of Figure 1 and part b of Figure 2) for the subsequent experiments.

TG (together with its derivative vs temperature, DTG) and DTA curves obtained during Nomex pyrolysis under

(15) Blazsó, M. *J. Anal. Appl. Pyrolysis* **1995**, *35*, 221.
(16) Mcneill, I. C.; Ahmed, S.; Memetea, L. *Polym. Degrad. Stab.* **1995**, *47*, 423.
(17) Setnescu, R.; Jipa, S.; Stenescu, T.; Kappel, W.; Kobayashi, S.; Osawa Z. *Carbon* **1999**, *37*, 1.
(18) Dubois M.; Naji, A.; Buisson, J. P.; Humbert, B.; Grivei, E.; Billaud, D. *Carbon* **2000**, *38*, 1411.
(19) Scarlete, M.; Butler, I. S.; Harrod, J. F. *Chem. Mater.* **1995**, *7*, 1214.
(20) Mokhtari, M.; Park, H. S.; Roesky, H. W.; Johnson, S. E.; Bolse, W.; Conrad, J.; Plass, W. *Chem.—Eur. J.* **1996**, *2*, 1269.
(21) Hamilton, K. E.; Letts, S. A.; Buckley, S. R.; Fearon, E. M.; Wilemsky, G.; Cook, R. C.; Schroen-Carey, D. *Fusion Technol.* **1997**, *31*, 391.
(22) Göschel, U.; Walter, H. *Langmuir* **2000**, *16*, 2887.
(23) Magonov, S. N.; Whangbo, M.-H. *Surface Analysis with STM and SEM*; VCH: Weinheim, 1996.
(24) Magonov, S. N.; Reneker, D. H. *Annu. Rev. Mater. Sci.* **1997**, *27*, 175.
(25) Bottomley, L. A. *Anal. Chem.* **1998**, *70*, 425R.
(26) Jandt, K. D. *Mater. Sci. Eng., R* **1998**, *21*, 221.
(27) Lillehei, P. T.; Bottomley, L. A. *Anal. Chem.* **2000**, *72*, 189R.
(28) Hamilton, L. E.; Gatewood, B. M.; Sherwood, P. M. A. *Text. Chem. Colorist* **1994**, *26*, 39.
(29) Zhong, Q.; Inniss, D.; Kjoller, K.; Elings, V. B. *Surf. Sci.* **1993**, *290*, L688.
(30) Tamayo, J.; García, R. *Langmuir* **1996**, *12*, 4430.
(31) Paredes, J. I.; Martínez-Alonso, A.; Tascón, J. M. D. *J. Mater. Chem.* **2000**, *10*, 1585.
(32) Magonov, S. N.; Cleveland, J.; Elings, V.; Denley, D.; Whangbo, M.-H. *Surf. Sci.* **1997**, *389*, 201.

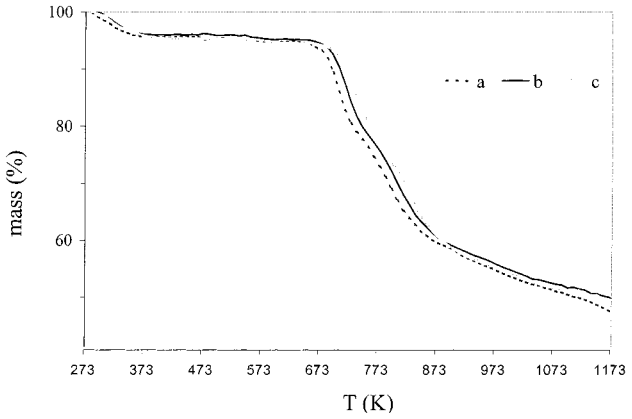

Figure 1. TG curves for heat treatments of Nomex under argon atmosphere using heating rates of 5 (a), 10 (b), and 20 K min^{-1} (c).

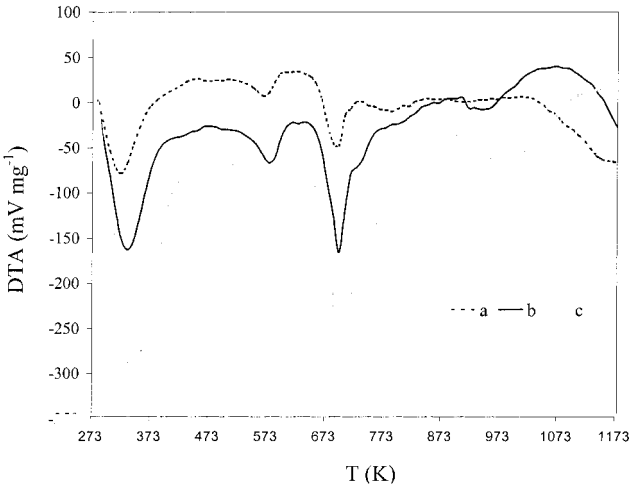

Figure 2. DTA curves for heat treatments of Nomex under argon atmosphere using heating rates of 5 (a), 10 (b), and 20 K min^{-1} (c).

argon with a heating rate of 10 K min^{-1} are shown in Figure 3. The first mass loss observed in the TG curve, which spans from room temperature to 378 K and is accompanied by an endothermal effect in the DTA curve with minimum at 333 K, is ascribable to the release of adsorbed moisture. No further changes occur until 543 K. The transformation undergone by the sample at this temperature is barely noticeable by a mass loss of approximately 1 wt % recorded in the TG curve, but it is highlighted in the DTG curve and also appreciated as an endothermal DTA peak with minimum centered at 590 K.

The major mass loss starts at approximately 673 K. Two steps are observed in the TG curve in the temperature ranges 673−753 and 753−873 K. For the DTA results, there is a well-defined endothermal peak with minimum at 700 K, located in the middle of the first mass loss step. However, the peaks are not well defined in the temperature range corresponding to the second TG step, suggesting that endothermal and exothermal effects are superimposed. From 873 K on, the TG curve shows a small but continuous mass loss which persists even at 1173 K, accompanied by an exothermal effect in the DTA curve.

The samples studied by FTIR and AFM were chosen and prepared to be representative of the different stages

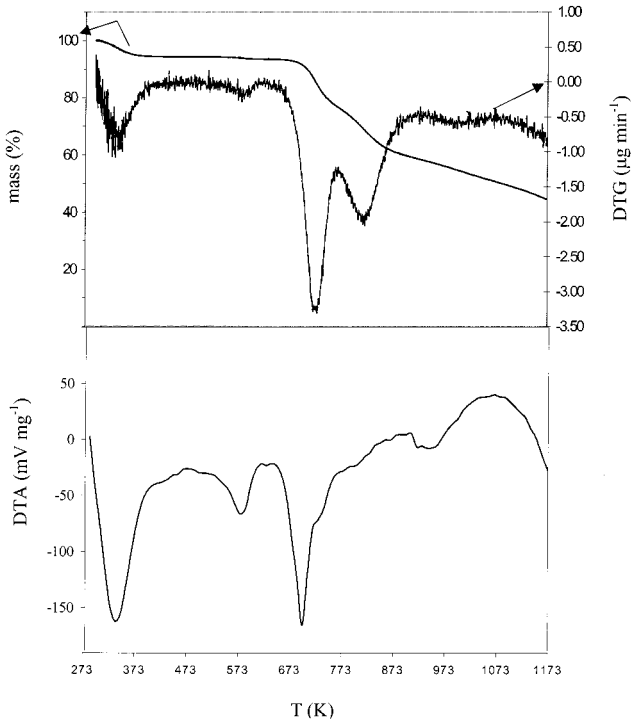

Figure 3. TG, DTG, and DTA curves for Nomex pyrolysis under argon with a heating rate of 10 K min^{-1}.

Table 1. Chemical Analyses of Fresh and Decomposed Nomex at Various Temperatures

T (K)	C (wt %)	H (wt %)	O (wt %)	N (wt %)	C (atom %)	H (atom %)	O (atom %)	N (atom %)
293	71.2	3.9	15.6	9.7	51.6	33.9	8.4	6.0
473	69.7	4.7	16.2	9.5	47.7	38.5	8.3	5.6
633	69.8	4.1	15.7	9.6	50.2	35.4	8.5	5.9
706	71.9	4.0	13.7	9.8	52.1	34.3	7.5	6.1
725	69.5	4.1	13.9	9.5	50.8	35.6	7.6	6.0
773	73.9	3.8	10.7	10.0	54.3	33.5	5.9	6.3
823	76.5	4.1	6.3	10.2	53.0	35.3	3.4	6.3
858	78.4	3.6	5.1	10.0	58.6	32.2	2.9	6.4
923	79.8	3.5	5.8	9.0	60.0	30.9	3.3	5.8
1023	80.4	2.2	7.4	7.0	67.8	22.4	4.7	5.1
1173	83.6	1.4	8.0	6.7	74.5	15.1	5.4	5.1

of pyrolysis as evidenced by the thermal analysis results.

3.2. Chemical Evolution during Pyrolysis: Elemental Analysis and Infrared Spectroscopy Measurements. The analyzed elements (C, H, O, N) when added together arrive at a total of 100 wt % within the experimental error. Thus, the starting material does not contain inorganic impurities in detectable quantity. This is confirmed by the fact that Nomex leaves no residue either after high-temperature oxidation in air or after low-temperature oxidation in a oxygen plasma. There is no significant change in the elemental composition of the sample until 823 K. From then onward, the sample gradually increases in its content of C, as expected in any carbonization process, while its atomic percentage of hydrogen decreases. The other heteroatoms, nitrogen and oxygen, are retained to a great extent. As a matter of fact, their atomic percent varies little during the whole process (Table 1).

The FTIR spectrum of fresh Nomex can be seen in Figure 4a and the main band assignments made in it are shown in Table 2. The spectra of samples treated

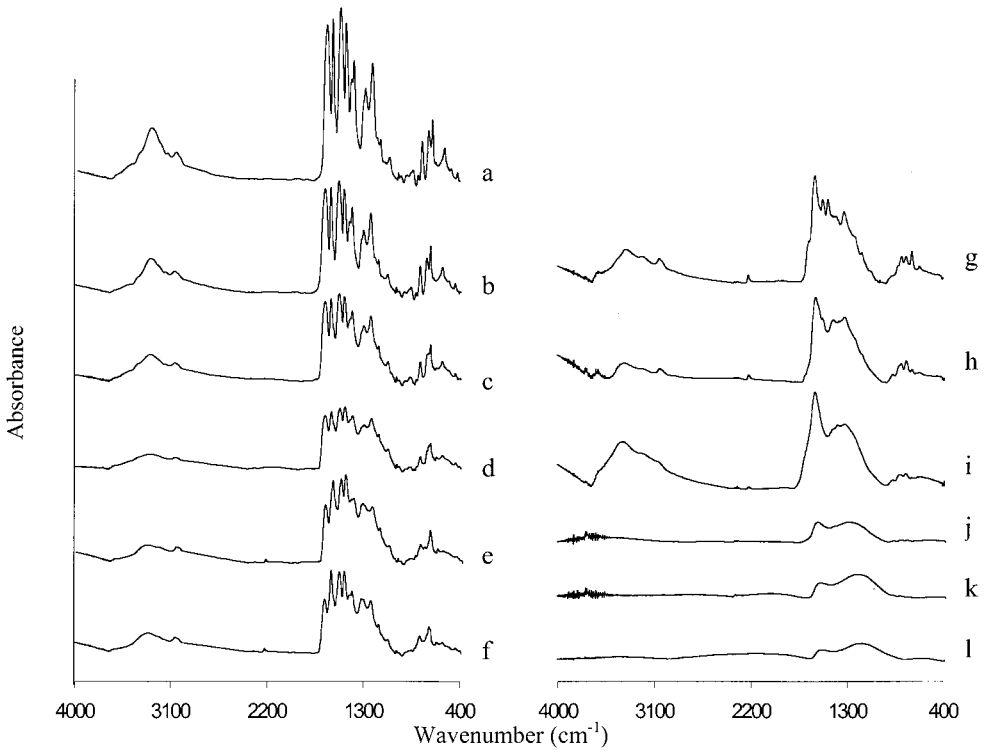

Figure 4. FTIR spectra of fresh Nomex (a) and its solid decomposition products at 633 (b), 706 (c), 746 (d), 803 (e) 823 (f), 873 (g), 923 (h), 973 (i), 1023 (j), 1073 (k), and 1173 K (l).

Table 2. FTIR Band Assignments in Fresh Nomex

wavenumber (cm^{-1})	band assignments
3300	N−H stretching vibrations in a secondary amide in trans form with a bonded hydrogen
3065	C−H stretching vibrations in an unsaturated compound
1660	amide C═O stretching (usually designated as amide I band) for hydrogen-bonded amide groups
1608	C═C stretching vibrations of aromatic ring
1536	N−H in-plane bending and C−N stretching coupled modes of the C−N−H group (also known as amide II band)
1305	aromatic C−N stretching
1240	C−N stretching, N−H in plane bending, C−C stretching (amide III)
781, 685	out-of-plane C−H vibrations of one and three adjacent hydrogens in a meta-substituted aromatic ring
720	N−H out-of-plane bending (amide V)

at temperatures 633−1173 K are shown in Figure 4(parts b−l). The spectrum of the sample heated to 633 K is virtually the same as that of the fresh sample except for a slight shift (∼10 cm^{-1}) to higher wavenumbers of the N−H stretching absorption band. As already mentioned, there is no remarkable change in the elemental composition of the sample until 823 K (Table 1) and so the number and position of the bands remain invariable through thermal treatments up to that temperature. The only exception is the appearance of an aryl nitrile band (2230 cm^{-1}) at 746 K. Consequently, it is possible to establish comparisons of peak intensities between the spectra of the fresh material and the samples in the 633−823 K temperature range. These comparisons are given in Table 3. The first column shows the ratio between the intensities of the amide C═O absorption band and the amide N−H band. As both bands correspond to the same chemical group, the quotient remains nearly constant through the entire process. The second column corresponds to the ratio between absorption intensities for the aromatic C═C band and the C−H band for the polymer. Again, this quotient remains reasonably constant in the mentioned temperature range. The third column gives the relative intensity between the bands corresponding to the aromatic C═C bonds and the amide C═O bonds, which remains constant up to temperatures of 746 K and increases at higher temperatures. Regarding the aryl nitrile, an increase in the intensity of its corresponding band is observed in the course of the degradation, as can be appreciated in Figure 4.

Table 3. FTIR Band Intensity Ratios at Various Decomposition Temperatures

T (K)	1660 cm^{-1}/ 3300 cm^{-1}	1608 cm^{-1}/ 3065 cm^{-1}	1608 cm^{-1}/ 1660 cm^{-1}
293	3.05	6.03	1.03
706	3.06	4.60	1.01
746	3.64	5.11	1.08
803	3.53	5.72	1.43
823	2.93	5.78	1.54

As the changes in the FTIR spectra at temperatures higher than 823 K are so great that the initial bands are severely altered, there is no point in making quantitative comparisons with the preceding spectra. As a consequence, results for these samples do not appear in Table 3. Above 873 K (Figure 4g), all the bands ascribed to the amide group disappear completely. In contrast, the peak centered at 1608 cm^{-1}, related to the aromatic bonds, persists and even broadens with increasing heat treatment temperature. The only FTIR

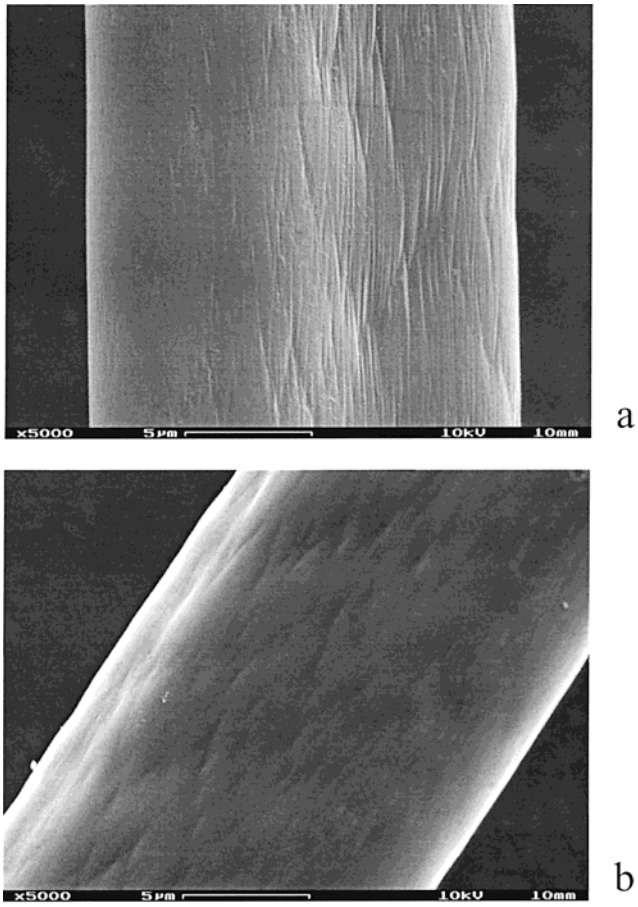

Figure 5. SEM micrographs of the Nomex fibers before and after pyrolysis: (a) fresh fiber, (b) final pyrolyzed fiber (1173 K).

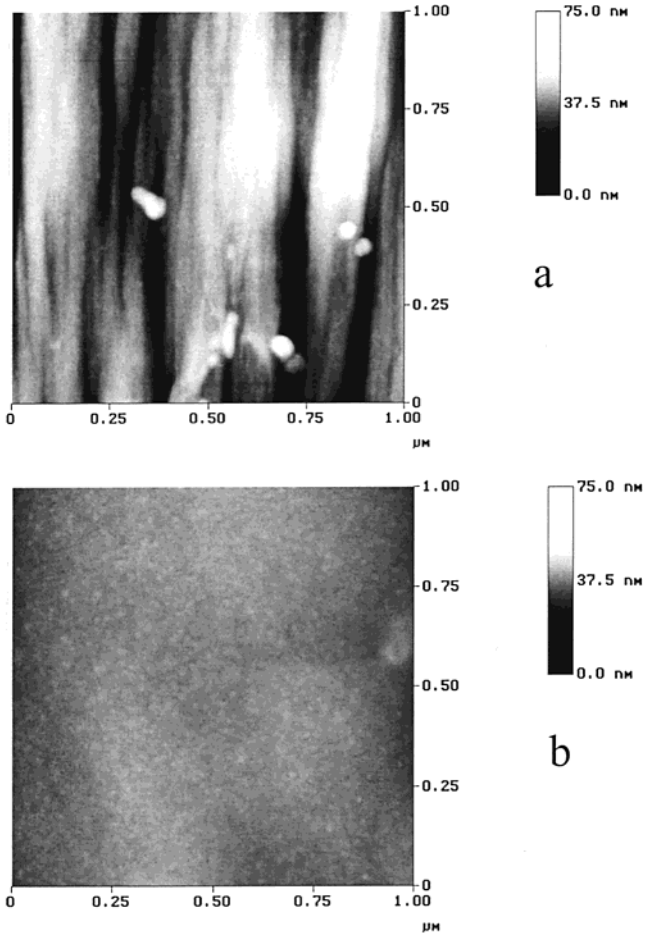

Figure 6. General appearance of Nomex fiber before and after pyrolysis. The images were obtained by tapping mode AFM: (a) fresh fiber, (b) fiber pyrolyzed at 1173 K. Lateral size: 1 μm.

spectrum of pyrolyzed Nomex found in the literature[8] corresponds to a sample that was heat-treated at 823 K for 15 min and is consistent with the spectra shown here, it being halfway between those corresponding to 823 and 873 K (spectra f and g of Figure 4). At 1023 K (Figure 4j), the aryl nitrile band has vanished as a consequence of the decomposition of this previously formed product. As indicated by the elemental analysis (Table 1), the atomic content of hydrogen significantly diminishes between 923 and 1023 K and this fact is reflected in the drop in intensity of the N−H and C−H stretching bands in the related spectra shown in Figure 4. Finally, at 1173 K (Figure 4l), the FTIR spectrum of the sample shows the typical absence of absorption bands of many carbonaceous materials.

3.3. Morphological Evolution during Pyrolysis: Atomic Force Microscopy Imaging. Before the AFM results for the different heat-treated samples are shown, it is interesting to present some SEM images for comparison. These were obtained using a Zeiss DSM-942 apparatus with samples that were gold-coated for electron conduction. Figure 5 shows typical SEM micrographs of the fresh Nomex fiber (a) and the fiber pyrolyzed at 1173 K (b). Both samples exhibit striations more or less parallel to the fiber axis, being apparently somewhat deeper and more numerous in the former case, which may indicate a general smoothing upon fiber degradation. Apart from this difference and from the fact that, as expected, a decrease in the diameter of the final pyrolyzed fiber as compared to that of the starting fiber (~16 vs 20 μm) is observed (arising from the consumption of a considerable portion of material at 1173 K), detailed morphological differences between the two fibers could not be detected at the magnifications that can be attained by SEM, and the same applied for the other heat-treated samples. If the fibers experience nanometer-scale morphological changes in the different steps of pyrolysis, they would be clearly detected only by AFM.

Figure 6 presents some AFM images comparing the general appearance of the same samples as in Figure 5. As can be seen, the difference between the starting material and the final carbonized fiber now becomes readily obvious. The former presents a morphology consisting of fibrils parallel to the fiber axis (from top to bottom in all the images presented here). These fibrils have typical diameters of a few tens of nanometers and are more or less arranged into groups separated by striations that are 50−100 nm wide and 20−30 nm deep. Most probably, some of the striations are those observed also by SEM (Figure 5a). By contrast, the fibrillar morphology has completely disappeared from the sample heat-treated at 1173 K. Now the topography turns out to be much smoother (root mean square roughness values of 1−3 nm compared to 7−10 nm for the untreated fiber), as also evidenced in the line profiles of Figure 7, and is characterized by approximately rounded platelets (which will be subsequently shown in

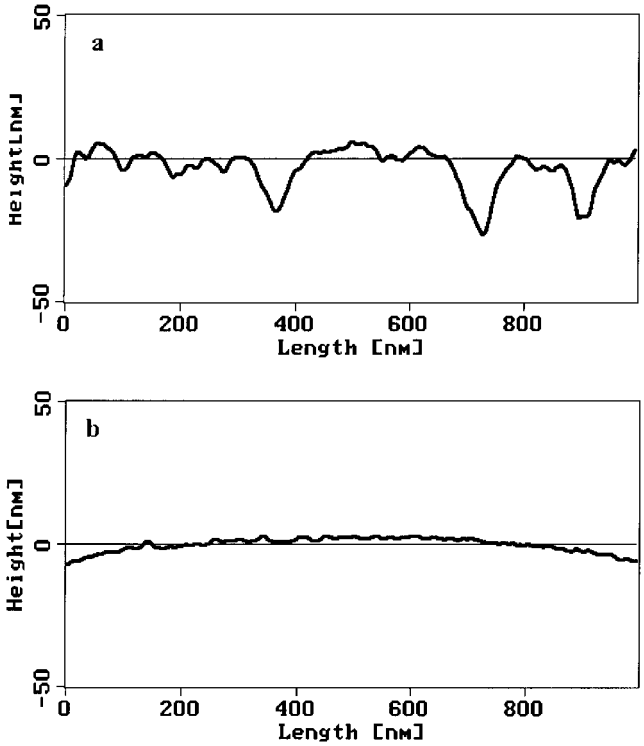

Figure 7. Line profiles of the fresh and pyrolyzed fibers from the images of Figure 6: (a) fresh fiber, (b) fiber pyrolyzed at 1173 K. The line profiles are drawn from left to right in the images, that is, perpendicular to the fiber axis.

more detail) typically between 10 and 20 nm in diameter. No preferred orientation of the features along the fiber axis can be evidenced now, in contrast to the fresh Nomex fiber. In consequence, the fiber surface has become more isotropic after the pyrolytic transformation.

In Figure 8, the detailed nanometer-scale evolution of the fiber surface morphology with heat treatment for selected temperatures, as detected by AFM, is shown. Although slight variations in the exact morphology could sometimes be observed from place to place within a given sample, the general features outlined in the images of Figure 8 were found to be representative of the changes undergone by the fibers upon heat treatment, since they reflected trends observed with a high reproducibility everywhere. As can be appreciated, there is a gradual transformation of the starting Nomex fiber (a) into the final fibrous carbon (f). Initially, as mentioned previously, the Nomex fiber presents a structure made up of long fibrils approximately parallel to the fiber axis (a reflection of its molecular conformation). Below the heat treatment temperature of 573 K, no appreciable changes in morphology are observed. After a heat treatment of 633 K (b), the anisotropy that is characteristic of the starting material has been lost to a noticeable extent and the long fibrils of the fresh fiber have been replaced by shorter features, as if the fibrils were truncated at several points, losing their long range (along the fiber axis) cohesiveness. Upon pyrolysis at 706 K (c), the anisotropy of the fiber has disappeared completely and its morphology consists of more or less rounded or elongated features with typical lateral sizes around 20 nm arranged in a disorganized way. Increasing the heat treatment temperature by 30 K, up to 736 K (d), results in a smoothing of the surface topography but the general features are quite similar to those of the previous sample, only perhaps they are now more rounded. After a heat treatment of 823 K (e), the fiber surface appears highly isotropic and is comprised of rounded domains (platelets) with diameters between 10 and 20 nm. This turns out to be, in essence, the final morphology of the pyrolyzed material, since no fundamental changes in the surface features take place by raising the heat treatment temperature to 1173 K (f), after which the aramid fiber has been thoroughly converted into fibrous carbon. The only difference observed is that in the final pyrolyzed sample, the features are somewhat more pronounced in the *z* direction than those in the 823 K sample, but basically, from a morphological point of view, the final carbonized material is already developed at this latter temperature.

It should also be noted that in the particular case of the 1173 K sample, further evidence of its morphology could be obtained from scanning tunneling microscopy (STM). The images recorded by STM were totally consistent with those acquired by AFM: rounded nanometer-sized features and absence of directionality along the fiber axis. For the rest of the samples, due to a lack of conductivity, STM imaging was not practicable because the tip would crash onto the samples.

4. Discussion

From the results presented in this work, several observations regarding the mechanisms of the thermal transformation of the Nomex fiber into fibrous carbon can be made. The first step in the process of the thermal degradation takes place at about 633 K with the cleavage of the hydrogen bonds that hold the polyaramide chains together. This breaking of the hydrogen bonds in Nomex is reflected in the endothermal effect registered in its DTA curve and also in the small mass loss (∼1%) recorded in the TGA curve (Figure 3) due to the release of water present in the crystalline lattice,[9] which was most probably forming hydrogen bonds with the amide groups. Evidence for the cleavage of the hydrogen bonds is also found in the FTIR spectra (Figure 4b): the shifting of the N−H amide band observed at 633 K (∼10 cm^{-1}) is characteristic of the breaking of this type of bond.[33] The AFM images at this temperature (Figure 8b) also reflect this change: as mentioned previously, the long fibrils typical of the pristine material have been replaced to a considerable extent by shorter features, without long range cohesiveness. This can be explained by the rupture of the hydrogen bonds, which leaves the polyaramide chains free to rearrange themselves, so that they curl up in a disorganized way when the sample is allowed to cool to room temperature. As a result, the chains lose their originally stretched arrangement and the anisotropy of the starting material is reduced.

The rupture of hydrogen bonds between polymer chains occurs prior to the main mass loss and is well differentiated from the onset of this process, which starts at 673 K and continues up to 873 K. In this range

(33) Brügel, W. *An Introduction to Infrared Spectroscopy*; John Wiley & Sons: New York, 1962.

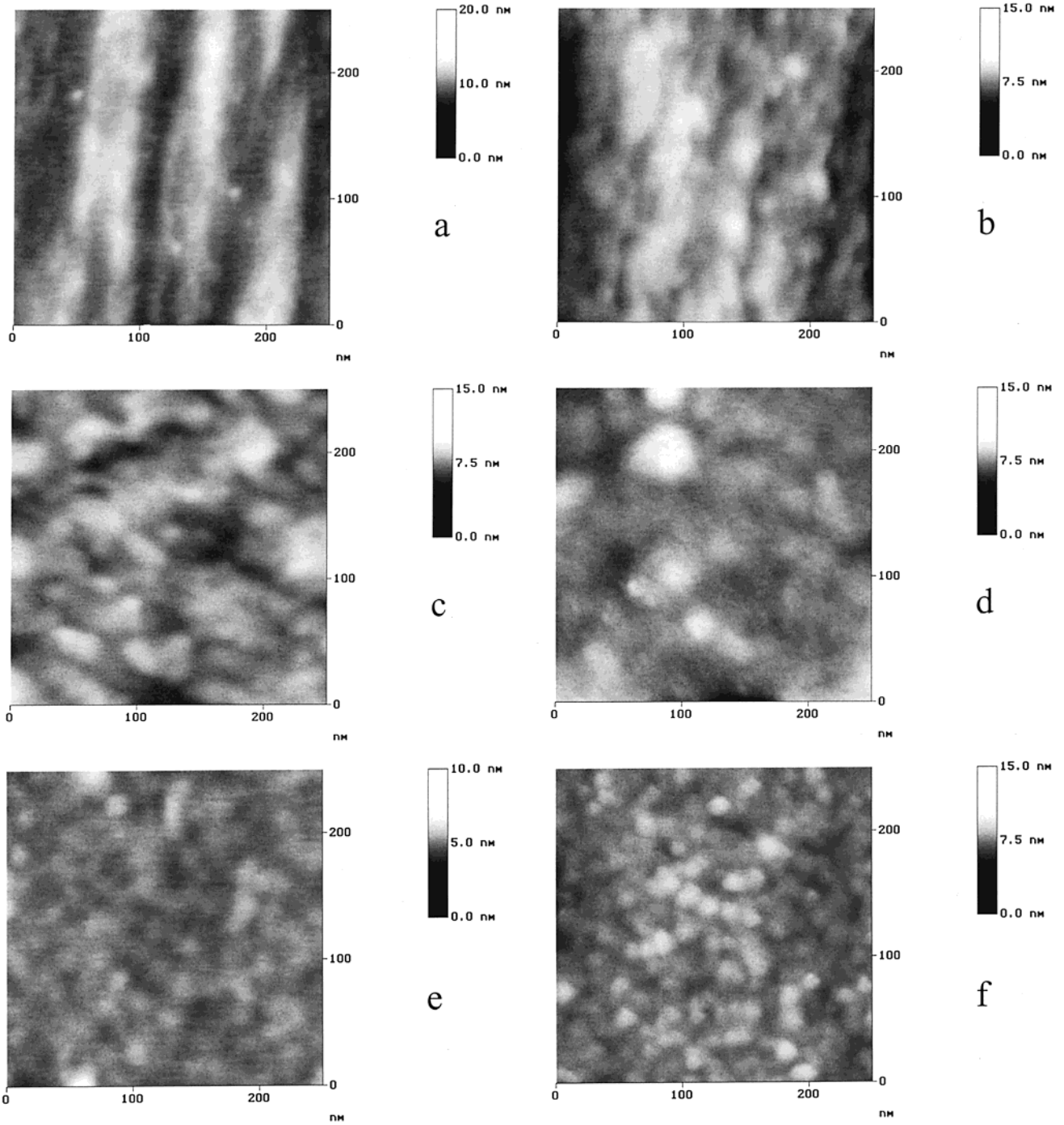

Figure 8. AFM images of the surface morphological evolution of fresh Nomex (a) and its solid decomposition products at 633 (b), 706 (c), 736 (d), 823 (e), and 1173 K (f). Lateral size: 250 nm.

of temperatures, the second step in the polymer decomposition comes about. Now, the amide bonds, which hold the aromatic units together, begin to break down and, as a consequence, the polyaramide chain collapses and divides into shorter chains. The TG results (Figure 3) evidence the existence of two regimes for this step, as commented beforehand. The first one, between 673 and 753 K, reflects the heterolytic breaking of the amide bonds.[7,9] This is also noticed in the DTA curve (Figure 3), which shows an endothermal peak at 700 K. The second regime spreads between 753 and 873 K and arises from the homolytic rupture of the amide bonds. The FTIR results corroborate the splitting of this step into two regimes: while the intensities of the bands related to the amide group and the aromatic ring drop in parallel in the first regime, in the second, only the intensities of the former diminish (Table 3). This observation suggests the occurrence of both polycondensation reactions, which are exothermal processes, and homolytic ruptures of the amide bonds (endothermal) simultaneously, which leads to the superposition of the two effects in the DTA curve in the temperature range between 753 and 873 K. The polycondensation reactions give rise to an increasing aromatization of the heat-treated sample. As regards the products of the rupture of the amide bond, aryl nitrile compounds have been detected in the present work (2230 cm^{-1} band in the FTIR spectra, Figure 4) and also in previous

studies.[10,13] Concerning the AFM results, the breaking of the polyaramide chains into smaller units and the subsequent disorder brought about by this effect is reflected in a further reduction of anisotropy in the sample surface morphology (Figure 8c−e).

Polycondensation reactions continue after 873 K, when amide bonds have disappeared (Figure 4h). The polycondensation is reflected in the small but continuous mass loss observed in the TG curve for this temperature range and coincident with a DTA (Figure 3) exothermal effect and the decrease in the hydrogen content (Table 1). It is also manifested by the persistence of a broadened peak at 1608 cm^{-1} in the FTIR spectra corresponding to the aromatic absorption band. The AFM morphology seen here at a temperature of 1173 K has also been found for other disordered carbonized materials[34] and is made up of small stacks (∼6 nm[35]) of graphite-like layers. Finally, the relative similarity in morphology between the AFM images of the samples heat-treated at 823 and 1173 K should be drawn to attention: it strongly suggests a considerable aromatization of the former sample, in agreement with the DTA and FTIR observations. Thus, the general picture at this last stage of the degradation process is that the skeleton of the final carbonaceous material has already been developed to a considerable extent at 823 K and, essentially, the evolution of the fiber from that temperature up to the formation of the final fibrous carbon at 1173 K proceeds by the dehydrogenation of the aromatic structures to eventually form small graphite-like assemblies.

(34) Nysten, B.; Roux, J.-C.; Flandrois, S.; Daulan, C.; Saadaoui, H. *Phys. Rev. B* **1993**, *48*, 12527.

(35) Blanco López, M. C.; Martínez-Alonso, A.; Tascón, J. M. D. *Microporous Mesoporous Mater.* **2000**, *34*, 171.

5. Conclusions

FTIR and AFM have proved to be very valuable techniques for providing direct and complementary information on the thermal degradation of Nomex aramid fibers. The chemical and morphological changes observed by these two techniques were found to be consistent with each other: (a) The rupture of hydrogen bonds between polyaramide chains revealed by FTIR was also evidenced by an increasing disorganization and a noticeable reduction of anisotropy observed in the AFM images on the nanometer scale. (b) The disruption of the amide bonds which the FTIR spectra indicated, and the subsequent splitting of the chains into smaller units, led to a further reduction of anisotropy and increasing nanometer-scale morphological disorder, as AFM was able to show. (c) The early (823 K) signs of polycondensation reactions appearing in the FTIR spectra and the dehydrogenation which follows at higher temperatures were coherent with the similarity between AFM images at 823 K and higher temperatures, with this resemblance strongly suggesting the formation of polyaromatic compounds at the former temperature. The morphological changes detected by AFM upon the different stages of pyrolysis could also reveal helpful information in similar studies of thermal treatment/degradation of other polymers.

Acknowledgment. The authors thank their colleagues Javier Fernández and Celina Blanco (DuPont Asturias) for providing the Nomex sample. Financial support from CICYT (Project 1FD1997-1915) is gratefully acknowledged. We also acknowledge a predoctoral fellowship from the Spanish Ministry of Education awarded to S.V.-R.

CM001219F